Magnetic Control of a Simple Pendulum with a Moving Pivot Point

Atzampou, Panagiota; Meijers, Peter; Tsouvalas, Apostolos; Metrikine, Andrei

DOI
10.1088/1742-6596/2647/3/032010

Publication date
2023

Document Version
Final published version

Published in
Journal of Physics: Conference Series

Journal of Physics: Conference Series

PAPER • **OPEN ACCESS**

Magnetic Control of a Simple Pendulum with a Moving Pivot Point

Journal of Physics: Conference Series **2647** (2024) 032010 doi:10.1088/1742-6596/2647/3/032010

Magnetic Control of a Simple Pendulum with a Moving Pivot Point

Panagiota Atzampou, Peter Meijers, Apostolos Tsouvalas, Andrei Metrikine

Delft University of Technology, Stevinweg 1, 2628CN Delft, the Netherlands

E-mail: P.Atzampou@tudelft.nl

Abstract. The present study introduces a magnetic PD control technique for the case of a simple pendulum driven by a sinusoidal motion of its pivot. The results attained demonstrate a good control performance for all the excitation cases of pivot point motion considered. The motion of the mass of the pendulum is successfully attenuated even when the pivot excitation is at the natural frequency of the pendulum. Furthermore, a fixed desired position can be achieved with small error and no saturation of the actuation present at steady-state. The initial distance between the magnet and the mass that ensures an efficient motion control is derived analytically and is validated by numerical simulations. The magnetic control method proposed serves as promising foundation for a non-contact position control technique for offshore wind turbine installation purposes.

1. Introduction

Offshore Wind Turbines (OWT) are formidable means of energy harvesting and nowadays get installed by floating heavy lift vessels (operating under dynamic positioning) in ever deeper waters due to the increase in the energy demands [1]. For the improvement of the overall safety and efficiency of the installation operations, a plethora of motion compensation and position control techniques have been tested over the years. These include gripper frames for monopiles [2] and manually manipulated or active tugger line motion control systems to maintain the correct position of the hanging load [3]. Motion compensation during installation has also been introduced indirectly by means of motion control of the crane itself [4], crane cart motion manipulation [5] and heave compensation [6]. The aforementioned methods require some form of direct contact between the mechanical equipment and the payload as well as some human intervention. These requirements amplified by the small error installation tolerances and the intense offshore environment, highlight the paucity for a contactless position technique for the OWT installation.

The concept investigated here is based on the magnetic interaction between the hanging component and an electromagnetic actuator. To design and develop such a technique, a simplified version of the envisioned system was studied: a simple magnetically controlled pendulum. The motion control was realized by employing a modified proportional-derivative (PD) controller, which adjusted the intensity and polarity of the electromagnetic actuator. The aim of the control was to attenuate the effects of a prescribed pivot point motion and to maintain a desired fixed position. A numerical model was build and several cases of excitation and initial

magnet distances were considered. An important indicator for successful motion control was its efficiency, namely achieving low error and evading the saturation of the actuator. The main parameters required for high performance control were also identified.

The paper is structured as follows: Section 2 describes concisely the dynamic system and the control algorithm. In Section 3, the simulation results are demonstrated and a criterion for defining an efficient initial distance between the magnets is derived analytically for different disturbance case scenarios. Lastly, the conclusions drawn as well as the motivation for further study are presented in Section 4.

2. Methodology

2.1. Equation of motion of the magnetically controlled pendulum

The dynamic system consists of a simple pendulum with a mass M connected to a rigid rod of total mass m and length ℓ rotating around the pivot point. A permanent magnet (PM) was attached to the center of one side of the cubical mass, while an electromagnet (EM) was placed opposite to the PM such that the dipole moments of the magnets are aligned on the same axis. The system is externally excited through the action of the EM and a horizontal prescribed motion of the pivot point h. The configuration is presented schematically in Figure 1a and shows the global fixed axes (x_G, y_G) and the moving with the pivot axes (x, y) of the system as well as the positive assumed directions for the angular and linear displacements. The free body diagram of the system is given by Figure 1b and demonstrates the forces acting on the pendulum mass. Due to the moving point of rotation, the motion of the mass of the pendulum is characterized by two horizontal displacements; one from the equilibrium position given by u (the unknown state of the system) and one derived from the global reference system $u_n = u + h$. The initial distance d and the time-variant separation distance $s = d - u_n$ between the EM and PM are defined in Fig. 1a. Table 1 demonstrates quantitatively important parameters of the set-up.

Table 1: Set-up dimensions.

ℓ [m]	M [kg]	m [kg]	Cube Size [mm]	PM Size [mm]	EM Size [mm]
1.04	0.9382	0.1868	70 x 70	Diameter = 15 Thickness = 3	Diameter = 65 Thickness = 35

For the further study of the dynamic behaviour of the system, the equation of motion (EOM) of a one degree-of-freedom pendulum is derived. It is assumed that the response of the system complies with the small angle approximation (namely $u = \ell\theta$ applies), and thus it is geometrically linearized around the equilibrium point. The EOM then reads:

$$\left(M + \frac{m}{3}\right)\ddot{u} + \left(M + \frac{m}{2}\right)\frac{g}{\ell}u = -\left(M + \frac{m}{2}\right)\ddot{h} + F + D, \tag{1}$$

where the gravitational acceleration g is taken to be equal to $9.81\,\mathrm{m/s^2}$, D pertains to the action of damping present at the hinge, F is the electromagnetic interaction force between the two magnets and the dot above a variable denotes a derivative with respect to time. The natural frequency of the system (f_n) is approximately equal to 0.496 Hz.

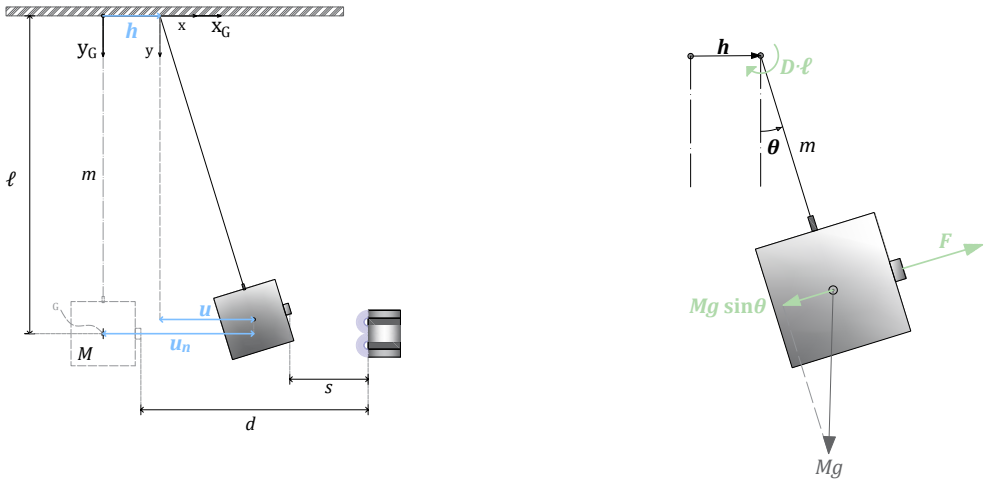

(a) Model set-up (b) Free body diagram

Figure 1: Schematics of the studied magnetic pendulum.

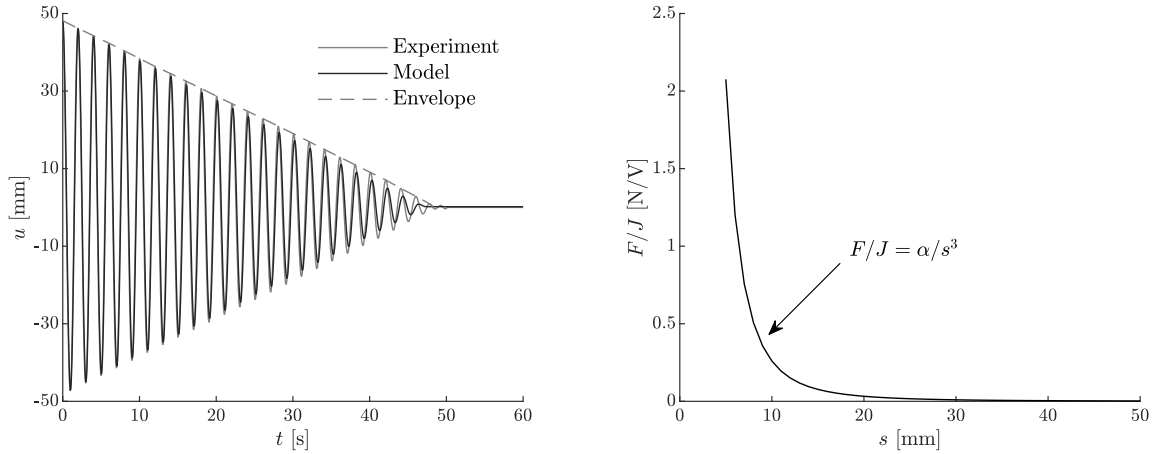

(a) Free vibration for initial distance $d = 50\,\text{mm}$ (b) Normalized magnetic force against separation s

Figure 2: Non-linear forces.

2.2. Damping Force

In the present work, the effective dissipative force D is described by Coulomb's friction formula:

$$D = \frac{M_{fr}}{\ell} = -\mu \,\text{sign}\,(\dot{u}), \tag{2}$$

where M_{fr} is the frictional moment at the hinge equal to $D\ell$ (Figure 1b), while μ governs the regime of the kinetic friction and upon experimental calibration was identified as $\mu = 0.005\,\text{N}$. In Figure 2a, experimental and model data are juxtaposed and the overall fit of the damping calibration is presented for the case of free vibrations.

2.3. Electromagnetic Force

The magnetic interaction between the two magnets is described by a representative formula, which was derived and calibrated using experimental data. The force generated by the EM is

$$F = \frac{\alpha J}{s^3}, \tag{3}$$

where s denotes the separation distance between the two magnets and it is defined as $s = d - u_n$. In Fig. 3, the magnetic interaction force is plotted against the relative distance s. The voltage output is defined as $J = RI$, where I denotes the current in the coil of the magnet, R the resistance of the circuit, while α is a model constant accounting for the strength of the PM, the strength and geometry of the EM. After calibration, the value of the constant was determined to be $\alpha = 2.5810 \times 10^{-7}\,\mathrm{Nm}^3/\mathrm{V}$. In order for the formula to be representative of the non-linear interaction, some tolerances needed to be respected. These tolerances refer to the margins of the initial distance and translate to $d \in [25, 75]\,\mathrm{mm}$.

As a result of the self-inductance L of the magnet, the current in the EM will not be proportional the supplied voltage $V(t)$. To account for this effect, the voltage output of the EM is modelled as an elementary RL circuit:

$$\dot{J} = \frac{1}{\tau}(V(t) - J), \tag{4}$$

in which $\dot{J}$ refers to the derivative of the voltage output with respect to time, while the time constant (delay) τ was extracted from measurement data and was identified as $\tau = 0.04\,\mathrm{s}$.

2.4. PD Control

A PD controller in time domain was considered in order to monitor and control the intensity of the electromagnetic interaction. The basic equation of a PD control variable in time domain is as follows:

$$c(t) = K_p e(t) + K_d \dot{e}(t), \text{with } e(t) = \delta(t) - u_n(t) = (\delta(t) - h(t)) - u(t), \tag{5}$$

where $c(t)$ represents the control variable, which refers to the voltage input of the electromagnet $V(t)$, and K_p and K_d represent the proportional and derivative gains of the PD control respectively. The error term $e(t)$ captures the divergence of the current measured global system's output $u_n(t)$ and the desired position $\delta(t)$.

Overall upon geometric linearization, the dynamical system has three main sources of non-linear behavior. These sources are the distance-dependent nature of the interaction force, the non-linear damping force as well as the physical saturation of the control system. As a result, alternative methods and modification for the control need to be considered. A potential linearization of the force generated by the EM (F) about the equilibrium would be unlikely to be fruitful, since such an approximation would significantly decrease the range of applicability of Equation (3) (the horizontal displacement bandwidth in which the excitation formula is able to predict the interaction force is reduced significantly). Thus, in order to work with a consistent linear case without jeopardizing the accuracy and representation of the electromagnetic interaction, an additional path was included into the control algorithm. This path, which bears a similarity with the non-linear control techniques of feedback linearization (§13, [7]) or gain scheduling (§12.5, [7]) was employed for the sole purpose of replacing the current non-linear controlled force with a linear control output for the PD control. More specifically, the control output $c(t)$ is multiplied by a correction factor γ, creating a new control output $c'(t)$.

$$c'(t) = K'_p(u(t))\, e(t) + K'_d(u(t))\, \dot{e}(t) \tag{6}$$

The modified PD controller has, thus, state dependent gains, i.e. $K'_p(u(t)) = \gamma K_p$, and $K'_d(u(t)) = \gamma K_d$, with $\gamma = s^3/\alpha$. Hereafter, this modification of the controller will be referred to as modified PD control. Due to the physical limits of the actuators performance, the new control output $c'(t)$ bears saturation limits associated with the input voltage capacities.

$$\mathrm{sat}(c'(t)) = \begin{cases} -24\,\mathrm{V} & \text{if } c'(t) < c'_{\mathrm{limit}^-} = -24\,\mathrm{V} \\ +24\,\mathrm{V} & \text{if } c'(t) > c'_{\mathrm{limit}^+} = +24\,\mathrm{V} \end{cases} \tag{7}$$

Furthermore, the assumption pertaining the delay (Equation (4)) between the voltage and the current intensity applied on the electromagnet was taken into consideration by including an additional step into the control loop. The modified PD control loop is presented in the block diagram in Figure 3.

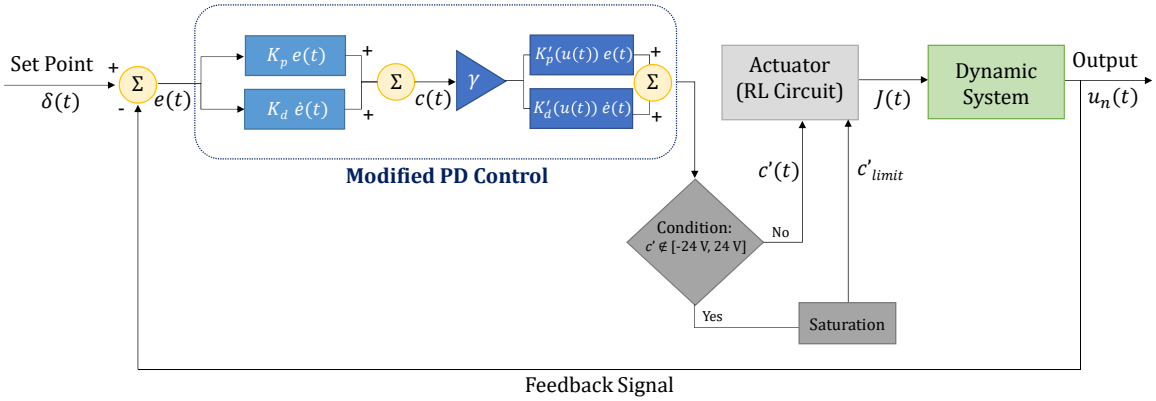

Figure 3: Block diagram for the modified PD control.

The updated EOM incorporated with the modified PD control is given as follows.

$$\left(M + \frac{m}{3}\right)\ddot{u} + \left(M + \frac{m}{2}\right)\frac{g}{\ell}u = -\left(M + \frac{m}{2}\right)\ddot{h} + c\,\mathrm{sign}\,(\dot{u}) + \frac{\alpha J}{s^3}, \tag{8a}$$

$$\dot{J} = \frac{1}{\tau}(c'(t) - J), \tag{8b}$$

$$c'(t) = \left[K'_p(\delta - u_n) + K'_d(\dot{\delta} - \dot{u}_n)\right]_{c'_{\mathrm{limit}^-}}^{c'_{\mathrm{limit}^+}} \tag{8c}$$

3. Results

3.1. Derivation of the critical initial distance

Due to the physical limits of the actuator and the tolerances introduced by the electromagnetic interaction (effective initial distance range without undesired sticking behaviour), a certain criterion can be set to predict the critical initial distance d_c to achieve an effective non-saturated controlled response. This critical distance could serve as a conservative criterion for high controllability (low error in the steady-state response and no saturation). Any initial distance value higher than d_c would result in a degree of saturation for the controller.

For simplification, the damping force and the self-impedance of the EM are omitted in the derivation of the critical d_c. After the aforementioned assumptions and the modified control output were applied, the EOM of the controlled system is given by

$$\left(M + \frac{m}{3}\right)\ddot{u} + \left(M + \frac{m}{2}\right)\frac{g}{\ell}u = -\left(M + \frac{m}{2}\right)\ddot{h} + K_p\,(\delta - h - u) + K_d\,(\dot{\delta} - \dot{h} - \dot{u}). \tag{9}$$

Equation (9) is a linear ordinary differential equation, which can be rewritten more concisely as

$$M_t\,\ddot{u} + K_t\,u = B\,\ddot{h} + K_p\,(\delta - h - u) + K_d\,(\dot{\delta} - \dot{h} - \dot{u}). \tag{10}$$

With this expression, the modified control output is given by the following expression,

$$c' = \gamma\left[K_p\,(\delta - h - u) + K_d\,(\dot{\delta} - \dot{h} - \dot{u})\right] = \gamma\,[M_t\,\ddot{u} + K_t\,u - B\,\ddot{h}], \tag{11}$$

with $\gamma = (d - u_n)^3/\alpha$. In the following, the motion of the pivot point is prescribed and equal to a harmonic sinusoidal motion with amplitude A and frequency ω, namely $h = A\sin(\omega t)$.

For this work, the desired motion δ is not a function of time but rather a constant desired position for the mass of the pendulum in the global reference frame. Hence, higher order derivatives of the desired motion are zero. Moreover, in order to define a criterion for effective control, two conditions need to be met. First, for the error of the control, $e \approx 0$ should apply, and, consequently, the steady state response of the pendulum can be approximated as $u \approx \delta - h$. After substitution of the first condition to Equation (11) and further simplifications one obtains

$$c' = \gamma\,[M_t\omega^2 A - K_t A + B\omega^2 A]\sin(\omega t) + \gamma\,K_t\delta, \tag{12}$$

with $\gamma = (d - \delta)^3/\alpha$. Second, there is a condition for effective control that pertains to the saturation and the limits of the control signal. Saturation occurs when the amplitude of the c' is equal to $c_{\text{limit}^\pm}$. As the amplitude of a pure sinusoidal signal is given by the factor in front of the sin function, this condition, if applied to Equation (12), yields

$$c_{\text{limit}^\pm} = \frac{(d-\delta)^3}{\alpha}\left[M_t\omega_c^2 A - K_t A + B\omega_c^2 A + K_t\delta\right], \tag{13}$$

where ω_c refers to the critical frequency above which the controller saturates partially or fully. Solving for the ratio of the critical frequency over the natural frequency of the system (ω_c/ω_n) gives the following closed form expression:

$$\frac{\omega_c}{\omega_n} = \sqrt{\frac{\frac{c_{\text{limit}^\pm}}{\gamma A K_t} + 1 - \frac{\delta}{A}}{1 + \frac{B}{M_t}}}. \tag{14}$$

In Equation (14), $1 + B/M_t$ is always a negative number as the coefficient $B < 0$. Thus, a physically-admissible critical frequency can only exist when

$$\frac{c_{\text{limit}^\pm}}{\gamma A K_t} + 1 - \frac{\delta}{A} < 0 \longrightarrow c_{\text{limit}^\pm} < \frac{(d-\delta)^3}{\alpha} K_t(\delta - A). \tag{15}$$

For the special case where the desired position is $\delta = 0$, a condition can be obtained for the critical initial distance d,

$$d < \sqrt[3]{\frac{\alpha\,\|c_{\text{limit}^-}\|}{K_t A}} = d_c, \tag{16}$$

where $\|c_{\text{limit}^-}\|$ signifies the absolute value of the physical limit of the electromagnet. Equation (16) can be graphically presented in Figure 4 for different excitation amplitudes and frequencies.

By calculating the d_c, one practically defines the optimum value for d for the static case of $\omega = 0$ rad/s and the maximum initial distance between the magnets without saturation. Figure 4 shows that the control is effective for an extensive range of excitation frequencies, in which the determining parameter is the initial distance. More specifically, for the range relevant for the application ($\omega/\omega_n \in [0, 4]$) and for low frequencies, this critical distance is almost constant or exhibits a small reduction of the order of approximately 5 mm, as shown in the inset in Figure 4. This figure can serve as indicator for a proper choice of d for successful control depending on the amplitude of the pivot motion.

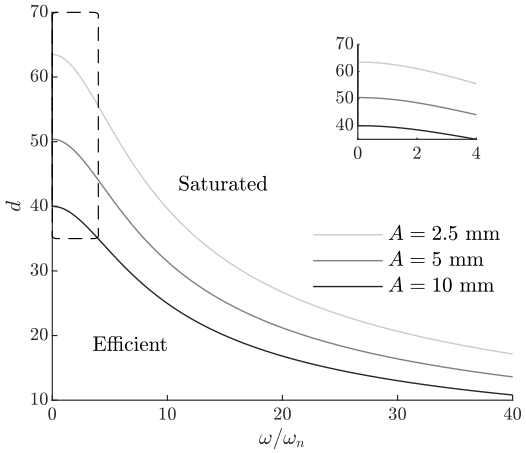

Figure 4: Critical distance d for the desired position $\delta = 0$. Saturation occurs in the area above the respective lines.

3.2. Times series of controlled motion

For a fixed desired position, $\delta = 0$, the time traces of the controlled motion as well as the respective control output are presented in Figure 5 for cases of excitation with amplitude $A = 5\,\text{mm}$ and different frequency ratios (ω/ω_n) for three initial distances d.

Overall, the controller succeeds in attenuating the externally-imposed motion caused by the pivot point and maintain the desired position regardless the excitation frequency. However, during the first few seconds of the response (during the transient), a large error is observed. As a result, the actuator operates at its limits in order to mitigate the motion. It is noted that the greater the initial distance, the longer the duration of and the higher the initial overshoot in the transient. Nevertheless, this part of the response is, from a broader perspective, short in duration (in the order of few seconds). Moreover, the values in error and saturation are considered acceptable to initiate an efficient control in this study. Therefore, the focus will be placed on the behaviour of the controlled system after the transient response is eliminated. In the steady state, a small fluctuation of the error is observed in all presented cases and the level of saturation depends on the initial distance. As shown in Figure 4, for amplitude $A = 5\,\text{mm}$ and for the the range of $\omega/\omega_n \in [0.6, 2.0]$, the control is successful without saturating for $d < 50\,\text{mm}$, which confirmed the validity of the criterion in Equation (14). There is a small tolerance for the critical value, where the control of the system can still be efficient despite being fully saturated. This is evident for the case of $d = 50\,\text{mm}$ in Figure 5, validating that the prediction of Equation (16) is rather conservative, as expected with respect to the assumptions made (absence of damping and EM self-inductance).

Figure 6 compares the controlled and uncontrolled response of the system to assess the overall efficiency of the motion compensation technique. The uncontrolled response corresponds to the motion of the system due to the applied pivot point excitation in absence of an electromagnet. By comparing this response to the controlled one, it is evident that significant motion mitigation is achieved even for this high value of excitation amplitude. As established from Figure 4, for the amplitude of $A = 10\,\text{mm}$, the initial distance of $d = 50\,\text{mm}$ provides an insufficient controllability. This specific case demonstrates exemplary behaviour of the system when the controller is fully saturated i.e. the control output is a square wave with an absolute amplitude equal to the capacity of the magnet. When the system is excited with its natural frequency (Figure 6b), the controller is able to prevent the system from exhibiting resonance and suppresses instability for $d < 50\,\text{mm}$.

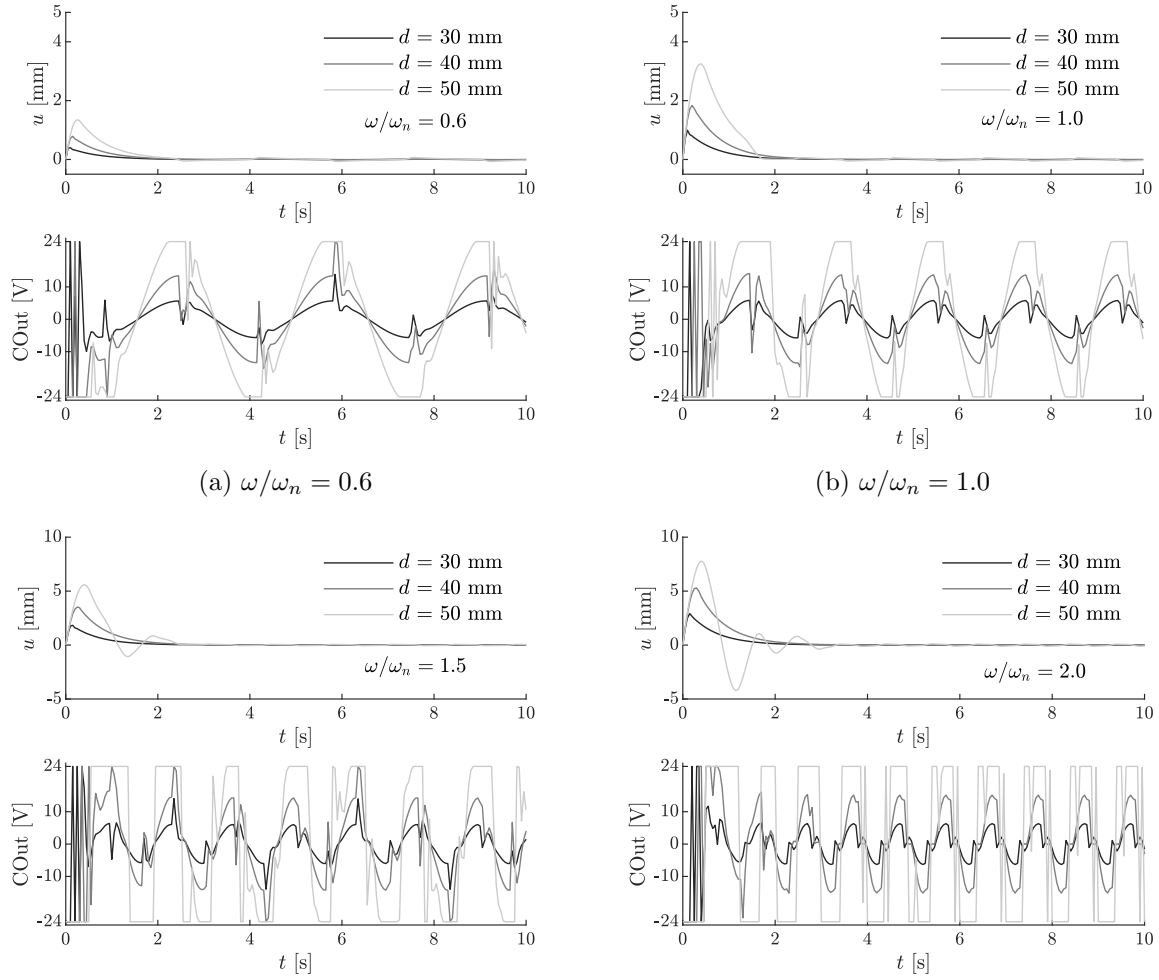

(a) $\omega/\omega_n = 0.6$ (b) $\omega/\omega_n = 1.0$

(c) $\omega/\omega_n = 1.5$ (d) $\omega/\omega_n = 2.0$

Figure 5: Displacement and control output time series of controlled motion for a harmonic excitation with $A = 5\,\text{mm}$ and desired position $\delta = 0$ for different initial separation distances d.

4. Conclusion

In this study, a contactless motion control technique was developed for the case of a magnetic simple pendulum with a moving pivot point. The technique was based on the magnetic interaction between two magnets, a permanent magnet and an electromagnetic actuator. The system was excited by an external harmonic motion of the pivot point and a desired position was imposed through a modified PD controller. The desired position was a fixed point in the global frame of reference. The results from the numerical simulation demonstrated that the controller is successful. However, the importance of a proper choice of the initial distance is highlighted. An expression for the critical initial distance is derived to ensure high performance of the controller for a single amplitude and a range of frequencies of excitation. High control performance corresponds to low deviation from the desired position and absence of saturation of the actuator. For a certain low range of frequency ratios ($\omega/\omega_n < 4$), the critical distance has an almost constant value. In terms of motion attenuation, the comparison of the controlled and uncontrolled response shows that the motion compensation is effective even at resonance.

In short, the contactless controller succeeds in maintaining a desired fixed position while

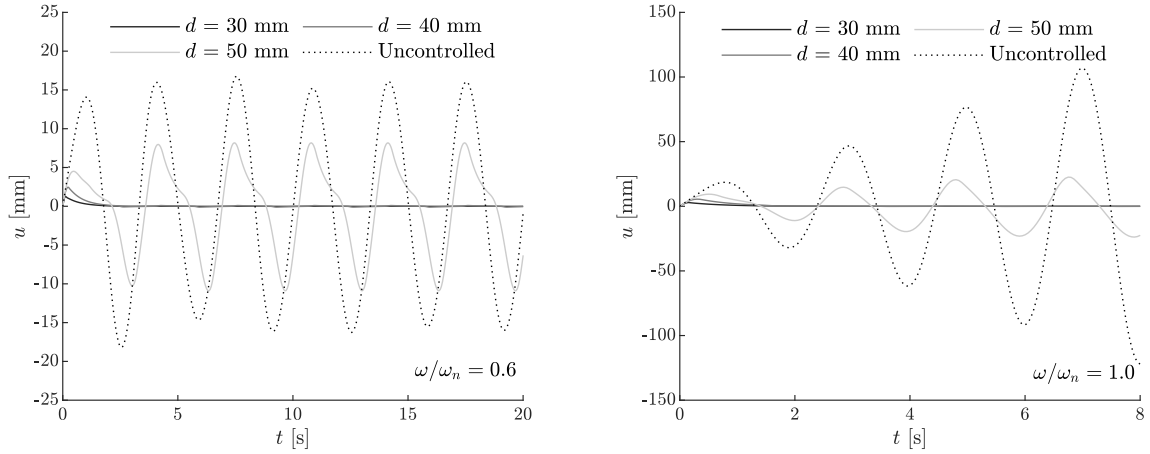

(a) $\omega/\omega_n = 0.6$ (b) $\omega/\omega_n = 1.0$

Figure 6: Comparison of the motion between the controlled and uncontrolled response for different initial distances d and a harmonic excitation amplitude $A = 10\,\text{mm}$.

mitigating the motion of the magnetic pendulum imposed by external pivot disturbance. The findings of this work underline the potential for the further advancement of this contactless motion control technique, and the eventual design of a more intricate multi-degree control algorithm for offshore applications.

References

[1] *Wind energy in Europe: 2021 Statistics and the outlook for 2022-2026 — WindEurope*. URL: https://windeurope.org/intelligence-platform/product/wind-energy-in-europe-2021-statistics-and-the-outlook-for-2022-2026/.

[2] Zhiyu Jiang. "Installation of offshore wind turbines: A technical review". In: *Renewable and Sustainable Energy Reviews* 139 (Apr. 2021), p. 110576. ISSN: 1364-0321. DOI: 10.1016/J.RSER.2020.110576.

[3] Zhengru Ren, Zhiyu Jiang, Zhen Gao, and Roger Skjetne. "Active tugger line force control for single blade installation". In: *Wind Energy* 21 (12 Dec. 2018), pp. 1344–1358. ISSN: 10991824. DOI: 10.1002/WE.2258.

[4] Shenghai Wang, Yuqing Sun, Haiquan Chen, and Jialu Du. "Dynamic modelling and analysis of 3-axis motion compensated offshore cranes". In: *Ships and Offshore Structures* 13 (3 Apr. 2017), pp. 265–272. ISSN: 17445302. DOI: 10.1080/17445302.2017.1360981.

[5] W. O'Connor and H. Habibi. "Gantry crane control of a double-pendulum, distributed-mass load, using mechanical wave concepts". In: *Mechanical Sciences* 4 (2 2013), pp. 251–261. ISSN: 2191916X. DOI: 10.5194/MS-4-251-2013.

[6] Jörg Neupert, Tobias Mahl, Bertrand Haessig, Oliver Sawodny, and Klaus Schneider. "A heave compensation approach for offshore cranes". In: *Proceedings of the American Control Conference* (2008), pp. 538–543. ISSN: 07431619. DOI: 10.1109/ACC.2008.4586547.

[7] Hassan K Khalil. *Nonlinear Systems*. en. 3rd ed. Upper Saddle River, NJ: Pearson, Dec. 2001.